ELSEVIER

Journal of Nuclear Materials 249 (1997) 199–206

journal of nuclear materials

The crystal structure of ianthinite, $[U_2^{4+}(UO_2)_4O_6(OH)_4(H_2O)_4](H_2O)_5$: a possible phase for Pu^{4+} incorporation during the oxidation of spent nuclear fuel

Peter C. Burns [a,*], Robert J. Finch [b], Frank C. Hawthorne [c], Mark L. Miller [d], Rodney C. Ewing [d]

[a] *Department of Geology, University of Illinois at Urbana-Champaign, 245 Natural History Building, 1301 West Greet Street, Urbana, IL 61801, USA*

[b] *Argonne National Laboratory, Chemical Technology Division, 9700 South Cass Avenue, Argonne, IL 60439-4837, USA*

[c] *Department of Geological Sciences, University of Manitoba, Winnipeg, Man., Canada R3T 2N2*

[d] *Department of Earth and Planetary Sciences, University of New Mexico, Albuquerque, NM 87131-1116, USA*

Received 17 October 1996; accepted 6 June 1997

Abstract

Ianthinite, $[U_2^{4+}(UO_2)_4O_6(OH)_4(H_2O)_4](H_2O)_5$, is the only known uranyl oxide hydrate mineral that contains U^{4+}, and it has been proposed that ianthinite may be an important Pu^{4+}-bearing phase during the oxidative dissolution of spent nuclear fuel. The crystal structure of ianthinite, orthorhombic, $a = 0.7178(2)$, $b = 1.1473(2)$, $c = 3.039(1)$ nm, $V = 2.5027$ nm^3, $Z = 4$, space group $P2_1cn$, has been solved by direct methods and refined by least-squares methods to an R index of 9.7% and a wR index of 12.6% using 888 unique observed [$|F| \geq 5\sigma|F|$] reflections. The structure contains both U^{6+} and U^{4+}. The U^{6+} cations are present as roughly linear $(U^{6+}O_2)^{2+}$ uranyl ions (Ur) that are in turn coordinated by five O^{2-} and OH^- located at the equatorial positions of pentagonal bipyramids. The U^{4+} cations are coordinated by O^{2-}, OH^- and H_2O in a distorted octahedral arrangement. The Urϕ_5 and $U^{4+}\phi_6$ (ϕ: O^{2-}, OH^-, H_2O) polyhedra link by sharing edges to form two symmetrically distinct sheets at $z \approx 0.0$ and $z \approx 0.25$ that are parallel to (001). The sheets have the β-U_3O_8 sheet anion-topology. There are five symmetrically distinct H_2O groups located at $z \approx 0.125$ between the sheets of Uϕ_n polyhedra, and the sheets of Uϕ_n polyhedra are linked together only by hydrogen bonding to the intersheet H_2O groups. The crystal–chemical requirements of U^{4+} and Pu^{4+} are very similar, suggesting that extensive $Pu^{4+} \leftrightarrow U^{4+}$ substitution may occur within the sheets of Uϕ_n polyhedra in the structure of ianthinite. © 1997 Published by Elsevier Science B.V.

1. Introduction

Ianthinite is the only known uranyl oxide hydrate mineral that contains U^{4+}. It has been identified from numerous uraninite-bearing deposits [1–6], and it may play a key role in the paragenesis of the complex assemblage of uranyl minerals that form where uraninite has been exposed to oxidizing meteoric water [1,7]. Due to its rarity, its instability in the presence of oxygen, and the difficulty in obtaining pure specimens, the crystal structure of ianthinite has resisted solution.

Recently, there has been renewed interest in the paragenesis and structures of uranyl oxide hydrate minerals, particularly schoepite, ianthinite and becquerelite, as they not only occur as the secondary products of alteration of uraninite under oxidizing conditions [1,5,8], but are also prominent alteration phases in laboratory experiments on UO_2 and spent nuclear fuel subjected to oxidative dissolution [9–14]. Details of the occurrence of uranyl oxide hydrate minerals are an important test of the extrapolation of the results of short-term experiments to periods relevant to nuclear-waste disposal [15]. Moreover, they provide important constraints on models used to predict the long-term behavior of spent nuclear fuel [16]. Finch and Ewing [17] proposed that ianthinite may be an important Pu^{4+}-

* Corresponding author.

PII S0022-3115(97)00212-2

bearing host phase formed during the oxidative dissolution of spent nuclear fuel, and ianthinite may control Pu concentrations in U-saturated solutions under oxidizing conditions (cf., [10]). However, the details of the crystal structure are required to assess the likelihood of Pu^{4+} incorporation.

2. Occurrence and previous studies

Ianthinite was first described by Schoep [18] from the Shinkolobwe (Kasolo) uranium mine in Shaba, Congo. Unit-cell parameters were reported by Frondel and Cuttita [19]: $a = 0.717$, $b = 1.146$, $c = 1.520$ nm, and by Guillemin and Protas [4]: $a = 0.715$, $b = 1.152$, $c = 3.03$ nm. Schoep [18,20] proposed the composition $2UO_2 \cdot 7H_2O$; this was revised by Bignand [6], who showed that the mixed-valence synthetic phase $UO_{2.84} \cdot xH_2O$ is isostructural with ianthinite. Guillemin and Protas [4] determined the H_2O content of a sample of ianthinite, and assigned the formula $UO_2 \cdot 5UO_3 \cdot 10.56H_2O$. Cordfunke et al. [21] synthesized a phase with composition $UO_{2.86} \cdot 1.5H_2O$, which has an X-ray powder-diffraction pattern that is similar to that of ianthinte (PDF 23-1461), but which may have contained minor dehydrated schoepite, $UO_3 \cdot 0.8H_2O$. Infrared absorption data have been reported for ianthinite by Cejka and Urbanec [22].

Ianthinite occurs with uranyl oxide hydrate minerals such as becquerelite, $Ca[(UO_2)_6O_4(OH)_6](H_2O)_8$, schoepite, $[(UO_2)_8O_2(OH)_{12}](H_2O)_{12}$, and vandendriesscheite, $Pb_{1.57}[(UO_2)_{10}O_6(OH)_{11}](H_2O)_{11}$, and is always closely associated with primary uraninite, UO_{2+x} [1–3]. Other mineral associations include the uranyl carbonates rutherfordine, UO_2CO_3, and wyartite, $3CaO \cdot U^{4+}O_2 \cdot 6U^{6+}O_3 \cdot 2CO_2 \cdot 12–14H_2O$ [2].

The conditions of formation of ianthinite are not well characterized. Ianthinite may form due to incomplete oxidation of uraninite, although the growth of synthetic ianthinite requires partial reduction of U^{6+} in solution [6,21]. The range of stability for ianthinite in natural waters has been estimated by Taylor et al. [23], who calculated a limited stability field in U-saturated aqueous solutions at 25°C: $P_{H_2O} > 10^{-2.5}$, $10^{-50} < P_{O_2} < 10^{-30}$ (atm). The stability field of ianthinite decreases with increasing temperature and vanishes near 100°C, where it is replaced by α-U_3O_8 and β-$UO_2(OH)_2$ [23]; however, Taylor et al. [24] showed evidence for the formation of synthetic ianthinite during the oxidation of UO_2 at 200°C caused by the depletion of oxygen in sealed reaction vessels. Ianthinite commonly lines cavities within corrosion rinds on uraninite where oxygen may become depleted during uraninite oxidation [17]. The coexistence of ianthinite with uranyl carbonates may reflect anoxic or moderately reducing conditions coincident with elevated P_{CO_2} values caused by biologic respiration or decomposition [17].

Ianthinite is unstable in air at ambient conditions [2,21]. Ianthinite oxidizes to schoepite or metaschoepite without substantial strain [25]; however, specimens of completely oxidized ianthinite ('epi-ianthinite') are commonly polycrystalline (our unpublished results). The optical properties of ianthinite vary with the degree of oxidation (Table 1); e.g., $2V\alpha$ increases with increasing degree of oxidation. The color of partly oxidized crystals of ianthinite varies from reddish purple to amber–brown or green. Crystallo-

Table 1
Optical properties reported for ianthinite and related hydrated uranium(VI) oxy-hydroxides

α	β	γ	$2V_\alpha$	Color	Ref.
Ianthinite					
1.674	1.90	1.92	small	dark violet	[20]
'Epi-ianthinite' [a]					
1.695	1.730	1.790	~ 50°	reddish purple	[19]
1.70	1.79	1.793	small	yellow	[25]
Schoepite [b]					
1.690	1.714	1.735	not reported	sulfur or lemon yellow	[41]
not reported	not reported	not reported	89.3°	yellow	[18]
1.690	1.714	1.735	large	golden yellow	[42]
1.70_{calc}	1.720	1.735	75°	amber–brown	[26]
Metaschoepite [c]					
not reported	not reported	not reported	not reported	golden yellow	[26]
Paraschoepite [d]					
1.705	1.760	1.770	40°	golden yellow	[25]
1.700	1.750	1.770	not reported	yellow	[26]

[a] 'epi-ianthinite' is considered synonymous with schoepite, but it is probably metaschoepite [4].
[b] a.k.a., 'schoepite I' [26].
[c] a.k.a., 'schoepite II' [26].
[d] a.k.a., 'schoepite III' [26].

graphically oriented inclusions of ianthinite in schoepite may give rise to extraneous diffraction maxima in X-ray precession photographs and powder patterns, and inclusions of ianthinite may explain unusual schoepite diffraction-patterns, such as reported by Christ and Clark [26] and attributed by them to the mineral paraschoepite [27].

3. Experimental

The ianthinite crystal studied was extracted from sample CSM 91.62 that was collected from the Shinkolobwe (Kasolo) mine in Shaba, southern Congo, and obtained by us from the Colorado School of Mines Geology Museum. The sample consists of a coarsely crystalline matrix of intergrown schoepite, becquerelite, vandendriesscheite and ianthinite, in contact with altered uraninite. The specimen also contains veins of fine-grained soddyite and uranophane. The crystal used was adjacent to uraninite and surrounded by granular schoepite or metaschoepite, much of which may have formed due to the oxidation of pre-existing ianthinite, as suggested by dark inclusions within the yellow crystals of schoepite.

A thin cleavage fragment with dimensions 0.21 × 0.19 × 0.03 mm was removed from the sample and examined optically and by X-ray precession photography. Optical examination of the crystal showed no evidence for schoepite intergrowths as described by Schoep and Stradiot [25] and Frondel and Cuttita [19]; however, schoepite or metaschoepite is evident in $\{0kl\}$ precession photographs as faint diffuse diffraction spots parallel to c^*. The precession photographs confirmed orthorhombic symmetry. The crystal was mounted on a Nicolet $R3m$ automated four-circle diffractometer equipped with a graphite monochrometer and Mo–Kα X-radiation. Forty-five diffraction maxima were centered, and the unit-cell dimensions (Table 2) were refined by least-squares methods.

Data were collected using the ω scan-mode with a variable scan-rate proportional to the peak intensity; minimum and maximum scan-speeds were 4.0 and 29.3° 2θ/min, respectively. A total of 4147 reflections was measured over the range $4° \le 2\theta \le 60°$, with index ranges $0 \le h \le 10$, $0 \le k \le 17$, $0 \le l \le 43$. Two standard reflections were measured after every 58 reflections; no significant variation of the standard reflections occurred during data collection, indicating that the crystal was stable under the conditions of the data collection. One hundred and two reflections were discarded due to peak asymmetry and one due to bad backgrounds, leaving 4043 data. An empirical absorption–correction was applied, based on 36 psi-scans of each of 11 diffraction maxima at least every 5° from 7.6 to 51.5° 2θ. The crystal was modeled as a {001} plate, and 539 reflections with a plate-glancing angle of less than 6° were discarded. The value of 6° was arrived at by using a range of glancing angles and determining where the effect of varying the glancing angle produced no improvement in the refinement. The absorption correction reduced R(azimuthal) from 27.9% to 5.7%. Reflections were corrected for Lorentz, polarization and background effects.

Table 2
Miscellaneous information for ianthinite

Space group	$P2_1cn$	Crystal size (mm)	0.21×0.19×0.03
a (nm)	0.7178(2)	Total Ref.	4147
b (nm)	1.1473(3)	Unique $\lvert F\rvert \ge 5\sigma\lvert F\rvert$ [a]	888
c (nm)	3.039(1)	Final R	9.7
V (nm^3)	2.5027	Final wR	12.6
μ	388 cm^{-1}	D_{CALC}	5.00 g/cm^3
F(000)	3160		

Unit-cell contents: $4\{U_2^{4+}(UO_2)_4O_6(OH)_4(H_2O)_4](H_2O)_5\}$.
$R = \Sigma(|F_o| - |F_c|)/\Sigma|F_o|$
$wR = [\Sigma w(|F_o| - |F_c|)^2/\Sigma wF_o^2]$, $w = 1/\sigma^2(F)$.
[a] Observed reflections remaining after absorption correction.

3.1. Diffraction-peak overlap

Peak overlap was a significant problem for the data due to the relatively large unit-cell volume (2.502 nm^3) and long c axis (3.034 nm) of ianthinite. Data exhibiting peak overlap were evident from asymmetric background counts; only the worst of these were removed by the data-reduction program. Peak overlap commonly results in (erroneously) negative peak intensities due to background enhancement; however, not all peaks affected by overlap displayed negative intensities. Because the relatively large mosaic spread in the crystal contributes to peak broadening, we did not attempt to reduce peak overlap by narrowing the scan ranges; instead, peak intensities with asymmetric backgrounds were discarded following the data collection. All data for which left and right background (raw) counts differed by more than one σ of the integrated peak intensity (I_o) were deleted from the data set. Thus 359 reflections were removed.

4. Structure solution and refinement

Scattering curves for neutral atoms, together with anomalous-dispersion corrections, were taken from Cromer and Mann [28] and Cromer and Liberman [29], respectively. R indices are of the form given in Table 2 and are given as percentages. The Siemens SHELXTL PLUS (PC version) system of programs was used throughout this study.

A recognizable partial-structure model was obtained in the space group $P2_1cn$ using direct methods. The model included U positions as well as a few anion positions. Successive cycles of least-squares refinement followed by the calculation of difference-Fourier maps gradually re-

vealed additional anion positions. Difference-Fourier maps calculated parallel to (001) at $z = 0.125$ revealed five peaks attributable to interlayer H_2O groups. One of these peaks [$H_2O(9)$] was split into three roughly equal maxima separated by ~ 0.18 nm; an O atom with occupancy factor of 0.33 was placed on each of these peaks. The least-squares matrix was ill-conditioned because of the pseudo-symmetric arrangement of the U positions and the relatively poor parameter-to-data ratio; significant damping was necessary to obtain convergence. Some of the uranyl ion U^{6+}–O bond-lengths refined to unreasonably short values; they were subsequently constrained to be ~ 0.18 nm by adding extra weighted observational equations to the least-squares matrix. Full-matrix least-squares refinement of the model, which included positional parameters for all atoms, anisotropic-displacement parameters for the U positions, and overall isotropic-displacement parameters for the anion positions, converged to a final R index of 9.7% and a wR index of 12.6% for 888 observed reflections ($|F| \geq 5\sigma|F|$), although the displacement parameters for some of the atomic positions were poorly behaved (Table 3). The high R indices and poor displacement-factors reflect problems with the data which include peak overlap, weak intensities, possible crystal inclusions, and an imperfect absorption correction. Final atomic parameters are given in Table 3 and bond lengths are listed in Table 4.

Table 3
Atomic parameters for ianthinite

	x	y	z	U_{eq} *
U(1)	0.000	0.059(1)	0.0057(5)	427(21)
U(2)	0.012(3)	−0.249(1)	−0.0117(9)	732(23)
U(3)	0.013(3)	−0.558(1)	0.0077(5)	552(23)
U(4)	0.008(2)	−0.496(2)	0.2397(1)	50(5)
U(5)	0.005(4)	0.8140(9)	0.2567(6)	40(14)
U(6)	0.013(4)	0.1929(9)	0.2557(5)	11(10)
O(1)	0.083(5)	0.043(5)	0.061(2)	50(33)
O(2)	−0.016(5)	0.060(5)	−0.054(2)	50(33)
O(3)	0.000(5)	−0.522(4)	0.065(2)	50(33)
O(4)	0.008(5)	−0.593(5)	−0.050(2)	50(33)
O(5)	0.013(5)	0.764(4)	0.313(2)	50(33)
O(6)	0.002(5)	0.857(5)	0.200(2)	50(33)
O(7)	0.004(5)	0.218(5)	0.314(2)	50(33)
O(8)	0.008(5)	0.133(5)	0.201(2)	50(33)
O(9)	−0.169(5)	−0.111(5)	−0.004(3)	50(33)
O(10)	−0.166(5)	−0.420(5)	−0.020(3)	50(33)
O(11)	0.186(5)	−0.366(5)	0.240(4)	50(33)
O(12)	0.837(5)	−0.358(5)	0.241(4)	50(33)
O(13)	0.822(5)	−0.633(5)	0.244(4)	50(33)
O(14)	0.201(5)	−0.634(5)	0.238(4)	50(33)
OH(1)	0.198(5)	−0.128(5)	−0.046(3)	67(46)
OH(2)	0.009(5)	0.234(5)	0.034(3)	67(46)
OH(3)	0.213(5)	−0.377(5)	−0.040(3)	67(46)
OH(4)	0.057(5)	−0.013(5)	0.285(3)	67(46)
$H_2O(1)$	0.025(5)	−0.262(5)	−0.095(3)	142(45)
$H_2O(2)$	0.014(5)	−0.519(5)	0.163(3)	142(45)
$H_2O(3)$	−0.001(5)	−0.520(5)	0.317(3)	142(45)
$H_2O(4)$	0.013(5)	−0.236(5)	0.066(3)	142(45)
$H_2O(5)$	0.801(5)	0.910(5)	0.126(4)	142(45)
$H_2O(6)$	0.226(5)	0.890(5)	0.141(4)	142(45)
$H_2O(7)$	0.732(5)	0.090(5)	0.121(4)	142(45)
$H_2O(8)$	0.291(5)	0.120(5)	0.134(4)	142(45)
$H_2O(9a)$	0.670(5)	0.469(5)	0.130(5)	100
$H_2O(9b)$	0.858(5)	−0.470(5)	−0.128(5)	100
$H_2O(9c)$	0.006(5)	−0.598(5)	−0.130(5)	100

* $U_{eq} = U_{eq} \times 10^4$.

Table 4
Bond lengths (nm) for ianthinite

U(1)–O(1)	0.181(5)	U(4)–O(11)	0.196(5)
U(1)–O(2)	0.182(5)	U(4)–O(14)	0.211(5)
U(1)–O(9)	0.232(5)	U(4)–$H_2O(2)$	0.236(9)
U(1)–OH(2)	0.219(6)	U(4)–$H_2O(3)$	0.237(10)
U(1)–O(9) [a]	0.245(4)	U(4)–O(12) [f]	0.200(5)
U(1)–OH(1) [b]	0.260(6)	U(4)–O(13) [f]	0.207(5)
U(1)–OH(1)	0.301(6)	$<$U(4)–$\phi>$	0.214
$<$U(1)–$\phi_{eq}>$	0.251		
		U(5)–O(5)	0.180(5)
U(2)–O(9)	0.205(5)	U(5)–O(6)	0.178(5)
U(2)–O(10)	0.235(5)	U(5)–O(11) [g]	0.250(6)
U(2)–OH(1)	0.218(7)	U(5)–O(12) [h]	0.236(6)
U(2)–OH(3)	0.224(6)	U(5)–O(13) [i]	0.235(4)
U(2)–$H_2O(1)$	0.254(11)	U(5)–O(14) [i]	0.227(5)
U(2)–$H_2O(4)$	0.236(11)	U(5)–OH(4) [g]	0.219(6)
$<$U(2)–$\phi>$	0.229	$<$U(5)–$\phi_{eq}>$	0.233
U(3)–O(3)	0.178(5)	U(6)–O(7)	0.178(5)
U(3)–O(4)	0.180(5)	U(6)–O(8)	0.180(5)
U(3)–O(10)	0.220(6)	U(6)–OH(4)	0.254(6)
U(3)–OH(3)	0.292(7)	U(6)–O(11) [j]	0.245(5)
U(3)–O(10) [c]	0.234(4)	U(6)–O(12) [k]	0.240(5)
U(3)–OH(2) [d]	0.252(6)	U(6)–O(13) [l]	0.245(6)
U(3)–OH(3) [e]	0.248(6)	U(6)–O(14) [m]	0.246(6)
$<$U(3)–$\phi_{eq}>$	0.249	$<$U(6)–$\phi_{eq}>$	0.246

[a] $x + \frac{1}{2}$.
[b] $= x - \frac{1}{2}$.
[c] $= x + \frac{1}{2}$.
[d] $= x, y - 1, z$.
[e] $= x - \frac{1}{2}$
[f] $= x - 1, y, z$.
[g] $= x, y + 1, z$.
[h] $= x - 1, y - 1, z$.
[i] $= x - \frac{1}{2}, y + 1\frac{1}{2}, \frac{1}{2} - z$.
[j] $= x - \frac{1}{2}, y + \frac{1}{2}, \frac{1}{2} - z$.
[k] $= x + \frac{1}{2}, y + \frac{1}{2}, \frac{1}{2} - z$.
[l] $= x + 1, y + 1, z$.
[m] $= x, y + 1, z$.

5. Description of the structure

5.1. Uranium coordination

There are six symmetrically unique U positions in the structure of ianthinite. Where present in crystal structures, the U^{6+} cation is usually part of a nearly linear $(U^{6+}O_2)^{2+}$

uranyl ion [30] (designated Ur) with U^{6+}–O bond-lengths of ~ 0.18 nm. The uranyl ion occurs in structures coordinated by four, five or six anions, such that the coordinating anions and the U^{6+} cation are approximately coplanar, and the oxygen atoms that are part of the uranyl ions are the apices of square, pentagonal or hexagonal bipyramids.

Four of the six U positions in the structure of ianthinite contain a uranyl ion and thus correspond to U^{6+}: U(1), U(3), U(5) and U(6). In each case, the uranyl ion is coordinated by five equatorial anions in a roughly planar arrangement, resulting in pentagonal bipyramids (Fig. 1a). The uranyl ion U^{6+}–O bond lengths in the Urϕ_5 polyhedra (ϕ: O^{2-}, OH^-, H_2O) were constrained to be ~ 0.18 nm during the refinement of the structure. The O–U^{6+}–O bond angles of the uranyl ions, which were not constrained during the refinement, are U(1): 162(2); U(3): 176(2); U(5): 177(2) and U(6): 166(2)°. Based on a bond-valence analysis (see below), the U(1) and U(3) uranyl ions are each coordinated by two O atoms and three OH groups, and the $< U–\phi_{eq} >$ bond lengths are 0.251 and 0.249 nm, respectively, values which are in the range of $< U–\phi_{eq} >$ observed for Urϕ_5 polyhedra in well-refined structures [31]. The U(5) and U(6) uranyl ions are each coordinated by four O atoms and one OH group; the $< U–\phi_{eq} >$ bond lengths are 0.233 and 0.246 nm, respectively, values that are within the range expected for Urϕ_5 polyhedra [31].

The U(2) and U(4) sites are distinctly different from the other U sites. According to bond-valence sums (below), each is coordinated by four (O^{2-}, OH^-) anions and two H_2O groups in a distorted octahedral arrangement (Fig. 1b). The U(2)$O_2(OH)_2(H_2O)_2$ and U(4)$O_4(H_2O)_2$ polyhedra have $< U–\phi >$ bond-lengths of 0.229 and 0.214 nm, respectively. These two polyhedra do not contain a uranyl ion, suggesting that they are probably occupied by U^{4+}. The expected $^{[6]}U^{4+}$–O bond-length from sums of effective ionic-radii is 0.225 nm ($^{[6]}U^{4+} = 0.089$, $^{[3]}O^{2-} = 0.136$ nm [32]) whereas the $^{[6]}U^{6+}$–O bond length is 0.209 nm ($^{[6]}U^{6+} = 0.073$ [32]). The $< U(2)–\phi >$ bond-length of 0.229 nm is consistent with complete occupancy of the site by U^{4+}. The $< U(4)–\phi >$ bond length of 0.214 nm, however, is somewhat shorter than expected for an octahedron that contains only U^{4+}.

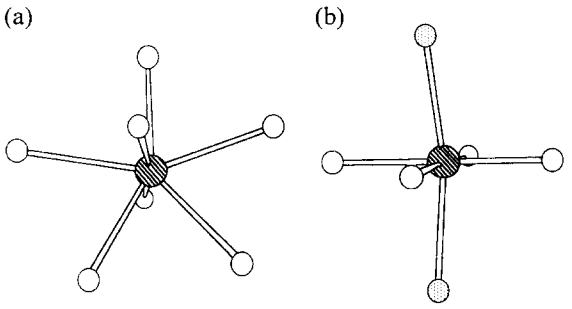

Fig. 1. Uranium-atom coordination geometries in the structure of ianthanite: (a) U(6)ϕ_7 pentagonal bipyramid (Urϕ_5), U(1), U(3) and U(5) have similar coordination polyhedra; (b) U(4)ϕ_6 distorted octahedron; U(2) has a similar coordination polyhedron. Uranium atoms: large circles shaded with parallel lines; O atoms and OH groups: open circles shaded; H_2O groups: circles shaded with a stippled pattern.

Table 5
Bond-valence [a] (vu) analysis for ianthinite

	U(1)	U(2)	U(3)	U(4)	U(5)	U(6)	Σ
O(1)	1.59						1.59
O(2)	1.55						1.55
O(3)			1.68				1.68
O(4)			1.62				1.62
O(5)					1.62		1.62
O(6)					1.68		1.68
O(7)						1.68	1.68
O(8)						1.62	1.62
O(9)	0.58, 0.45	1.04					2.07
O(10)		0.61	0.74, 0.56				1.91
O(11)				1.23	0.41	0.45	2.09
O(12)				1.14	0.54	0.50	2.18
O(13)				1.01	0.55	0.45	2.01
O(14)				0.94	0.64	0.44	2.02
OH(1)	0.34, 0.15	0.83					1.32
OH(2)	0.75		0.39				1.14
OH(3)		0.74	0.18, 0.43				1.35
OH(4)					0.75	0.38	1.13
H_2O(1)		0.43					0.43
H_2O(2)				0.60			0.60
H_2O(3)				0.59			0.59
H_2O(4)		0.60					0.60
H_2O(5)							0.00
H_2O(6)							0.00
H_2O(7)							0.00
H_2O(8)							0.00
H_2O(9)							0.00
Σ	5.41	4.25	5.60	5.51	6.19	5.52	

[a] Calculated using the parameters for U^{6+} given by Burns et al. [31].

5.2. Bond-valence analysis

A bond-valence analysis, calculated using the parameters for U^{6+} from Burns et al. [31], is presented in Table 5. The bond-valence analysis permits the identification of O^{2-}, OH^- and H_2O anions. The analysis gives cation bond-valence sums that are generally consistent with occupancy of the U(1), U(3), U(5) and U(6) sites by U^{6+} and occupancy of the U(2) site by U^{4+}. Calculating the bond-valence sum to the U(2) site using the bond-valence parameters given for U^{4+} by Brese and O'Keeffe [33] gives 4.05 vu, indicating that this site probably contains U^{4+}. The bond-valence sum of 5.51 vu for the U(4) site, obtained with the bond-valence parameters for U^{6+} [31], is much higher than the expected value of 4.0, whereas

calculating this sum using bond-valence parameters for U^{4+} [33] gives 6.02 vu. The higher-than-expected bond-valence sum at the U(4) position suggests that U^{5+} or U^{6+} may occur at this site. The electroneutrality principle requires that the U(4) site is occupied by a tetravalent cation; however, substitution of some U^{5+} or U^{6+} at the U(4) site could be locally charge-compensated by deprotonation of the H_2O groups that are bonded to U(4).

5.3. Structural formula of ianthinite

The determination of the exact formula of ianthinite from the present study is difficult owing to the poor quality of the data (due primarily to crystal problems) and the resulting large uncertainties in bond-lengths; thus the possibility of partial oxidation of U^{4+} to U^{5+} or U^{6+} cannot be ruled out. In fact, minor inclusions of the fully oxidized mineral schoepite in this crystal were indicated in the precession photographs, suggesting that partial oxidation is likely. The U(1), U(3), U(5) and U(6) sites are all occupied by U^{6+}, as shown by the presence of a uranyl ion. The U(2) and U(4) polyhedral geometries are approximately consistent with occupancy by U^{4+}. There are 22 distinct anion positions within the two structural sheets; arguments based upon bond valences indicate that there are 14 O atoms, 4 OH groups and 4 H_2O groups bonded within or directly to the two sheets. In addition, there are 5 H_2O groups between the sheets of $U\phi_n$ polyhedra. Thus, as each site is on a general position, the structure indicates that the formula of ianthinite is $[U_2^{4+}(UO_2)_4O_6(OH)_4(H_2O)_4](H_2O)_5$, where the square brackets enclose structural-sheet constituents. The ratio of U^{4+} to U^{6+} in ianthinite determined by us (2:4) is greater than that determined by Guillemin and Protas [4] from wet chemical techniques (1:5), although the total H_2O content is in reasonable agreement. However, the bond-valence arguments suggest that some U^{5+} or U^{6+} may occur at the U(4) site, reducing the total amount of U^{4+} in ianthinite. The calculated density from the structure refinement is 5.00 g/cm^3, which agrees reasonably well with the measured density of 5.16 ± 0.05 g/cm^3 [4].

5.4. Connectivity of the structure

A projection of the structure of ianthinite along [100] (Fig. 2) shows $U\phi_n$ polyhedra connected to form sheets parallel to (001). The only constituents that occur between the sheets of $U\phi_n$ polyhedra are H_2O groups. Thus, linkage between the sheets is by hydrogen bonds only. The data is not of sufficient quality to allow resolution of the H atom positions, as is usually the case for U phases.

There are two symmetrically distinct sheets of $U\phi_n$ polyhedra, one at $z \approx 0$ and the other at $z \approx 0.25$. Although symmetrically distinct, these sheets are topologically identical, as shown in Fig. 3. Each contains three unique U positions; two are associated with $Ur\phi_5$ polyhedra and one with a $U^{4+}\phi_6$ polyhedron. The sheets of $U\phi_n$ polyhedra result from sharing of corners and edges between $Ur\phi_5$ and $U^{4+}\phi_6$ polyhedra. $Ur\phi_5$ polyhedra share edges, forming chains parallel to x that are one $Ur\phi_5$ polyhedron wide; these chains are in turn linked together by the sharing of corners between $Ur\phi_5$ polyhedra of adjacent chains and by the sharing of edges with $U^{4+}\phi_6$ polyhedra located between the chains (Fig. 3a, b).

Representation of the sheet of $U\phi_n$ polyhedra (Fig. 3a, b) with its corresponding sheet anion-topology following the procedure of Burns et al. [34] results in the β-U_3O_8 anion-topology (Fig. 3c). The sheets in the structures of β-U_3O_8 [35] and billietite [36], $Ba[(UO_2)_3O_2(OH)_3]_2(H_2O)_4$, also have this anion topology. The sheets in the

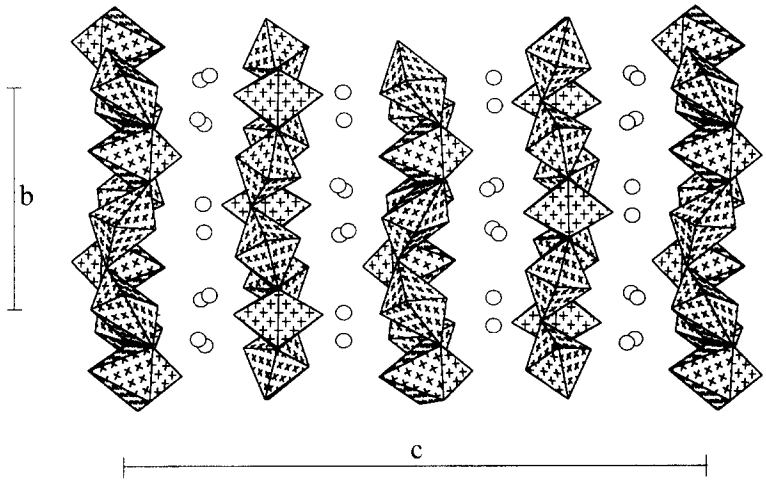

Fig. 2. The structure of ianthinite projected along [100]. The $U\phi_n$ polyhedra are shaded with crosses and H_2O groups of the interlayer are shown as open circles.

structure of β-U_3O_8 are linked by sharing O atoms between adjacent sheets, and there are no interlayer constituents. The structure of billietite contains two symmetrically distinct sheets of $U\phi_n$ polyhedra; one has the α-U_3O_8 anion-topology [34]; whereas, the other is more similar to the β-U_3O_8 anion-topology [34]. However, if the U(2)–O(5) bond-length of 0.302 nm is included in the latter sheet, it is better described as having the α-U_3O_8 anion-topology [34]. In the structure of billietite, the sheets of $U\phi_n$ polyhedra are linked by interlayer Ba cations and H_2O groups.

Schoepite is chemically similar to ianthinite, but it contains no U^{4+}. In air, ianthinite oxidizes to form schoepite [25]. The structure of schoepite was recently solved by Finch et al. [37]; their work showed that the structure contains sheets of $Ur\phi_5$ polyhedra (Fig. 4a) that are connected through hydrogen bonding to interlayer H_2O groups. The same sheet of $Ur\phi_5$ polyhedra also occurs in the structure of fourmarierite [38], $Pb[(UO_2)_4O_3(OH)_4](H_2O)_4$, and the topological arrangement of anions, referred to as the fourmarietite anion-topology [34] is shown in Fig. 4b. Note that the structure of ianthinite contains both $Ur\phi_5$ pentagonal bipyramids and distorted $U^{4+}\phi_6$ octahedra; whereas, the structure of schoepite contains only $Ur\phi_5$ pentagonal bipyramids.

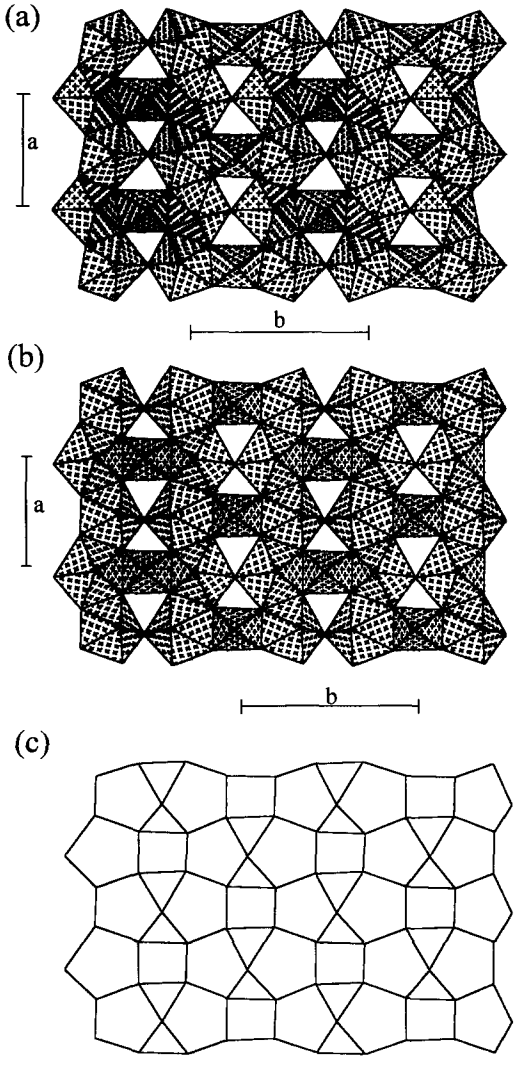

Fig. 3. The sheets of $U\phi_n$ polyhedra in the structure of ianthinite. Polyhedral representations of the sheets at: (a) $z \approx 0.0$ and (b) $z \approx 0.25$. The sheet anion-topology is shown in (c). Legend as in Fig. 2.

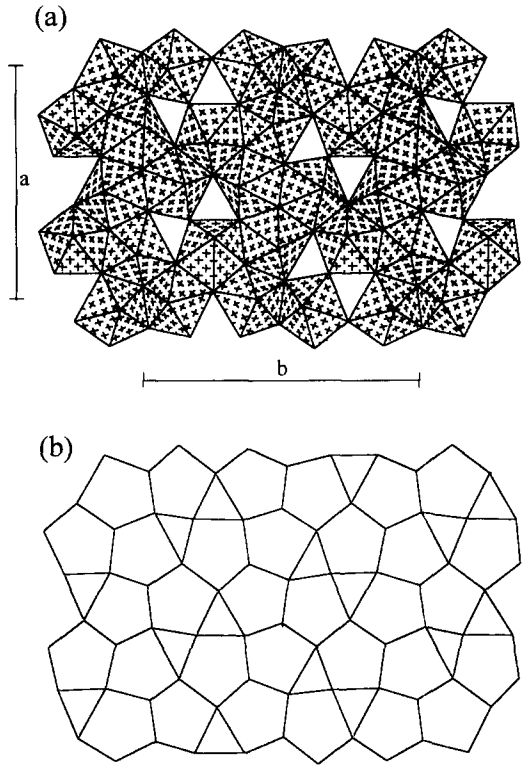

Fig. 4. The sheets of $Ur\phi_5$ polyhedra in the structure of schoepite: (a) polyhedral representation; (b) sheet anion-topology. Legend as in Fig. 2.

6. Incorporation of Pu^{4+} during the alteration of spent nuclear fuel

The structure of ianthinite is of considerable interest because it contains both U^{4+} and U^{6+}, and it, together with schoepite, is likely to form early during the oxidative dissolution of UO_2 in spent nuclear fuel. As such, Finch and Ewing [17] and Burns et al. [39] have proposed that the structure may be an important Pu^{4+}-bearing phase, and that it may possibly control Pu^{4+} concentration in U-saturated oxidizing solutions. The structure determination

presented here provides the basis to assess the possibility of Pu^{4+} incorporation into the structure of ianthinite.

The crystal–chemical requirements of Pu^{4+} are very similar to those of U^{4+}. Pu^{4+} is known to occur in coordination polyhedra with coordination numbers ranging from six to eight. The U^{4+} in the structure of ianthinite is in octahedral coordination, as is Pu^{4+} in the structure of $BaPu^{4+}O_3$ [40]. Bond lengths for $^{[6]}Pu^{4+}$–O and $^{[6]}U^{4+}$–O from sums of effective ionic-radii [32] are 0.222 and 0.225 nm, respectively. Thus, there is no structural limitation for the amount of $Pu^{4+} \leftrightarrow U^{4+}$ substitution that may occur in ianthinite, and a Pu-analogue of ianthinite with composition $[Pu_2^{4+}(UO_2)_4O_6(OH)_4(H_2O)_4](H_2O)_5$ could conceivably be stable. Thus, ianthinite may be an important Pu^{4+}-bearing phase during the oxidative dissolution of the UO_2 in spent nuclear fuel.

Acknowledgements

This work was supported by the Natural Sciences and Engineering Research Council of Canada in the form of Operating, Major Equipment and Infrastructure Grants to FCH and by a Post-Doctoral Fellowship to P.C.B. This work was also supported by the Office of Basic Energy Sciences (Grant No. DE-FG03-95ER14540).

References

[1] E.C. Pearcy, J.D. Prikryl, W.M. Murphy, B.W. Leslie, Appl. Geochem. 9 (1994) 713.
[2] M. Deliens, P. Piret, G. Comblain, Les Minéraux Secondaires d'Uranium du Zaïre (Musée Royal de l'Afrique Centrale, Tervuren, Belgium, 1981) 99 p.
[3] M. Deliens, Bull. Soc. Fr. Miner. Cristallogr. 100 (1977) 32.
[4] C. Guillemin, J. Protas, Bull. Soc. Fr. Miner. Cristallogr. 82 (1959) 80.
[5] C. Frondel, US Geol. Soc. Bull. 1064 (1958) 400.
[6] C. Bignand, Bull. Soc. Fr. Miner. Cristallogr. 78 (1955) 1.
[7] R.J. Finch, R.C. Ewing, Alteration of uraninite in an oxidizing environment and its relevance to the disposal of spent nuclear fuel, SKB Technical Report 91-15, SKB, Stockholm, 1991.
[8] R.J. Finch, R.C. Ewing, J. Nucl. Mater. 190 (1992) 133.
[9] L.H. Johnson, L.O. Werme, Mater. Res. Soc. Bull. XIX (12) (1994) 24.
[10] R.S. Forsyth, L.O. Werme, J. Nucl. Mater. 190 (1992) 3.
[11] D.J. Wronkiewicz, J.K. Bates, T.J. Gerding, E. Veleckis, B.S. Tani, J. Nucl. Mater. 190 (1992) 107.
[12] S. Stroes-Gascoyne, L.J. Johnson, P.A. Beeley, D.M. Sellinger, in: Scientific Basis for Nuclear Waste Management IX, Materials Research Society Proceedings, Vol. 50, ed. L.O Werme (Materials Research Society, Pittsburgh, PA, 1985) pp. 317.
[13] R. Wang, J.B. Katayama, Nucl. Chem. Waste Manag. 3 (1982) 83.
[14] T. Wadsten, J. Nucl. Mater. 64 (1977) 315.
[15] R.C. Ewing, in: Scientific Basis for Nuclear Waste Management XVI, Materials Research Society Proceedings, Vol. 294, eds. C.G. Interante and R.T. Pabalan (Materials Research Society, Pittsburgh, PA, 1993) p. 559.
[16] J. Bruno, I. Casas, E. Cera, R.C. Ewing, R.J. Finch, W.O. Werme, in: Scientific Basis for Nuclear Waste Management XVIII, Materials Research Society Proceedings, Vol. 353, eds. T. Murakami and R.C. Ewing (Materials Research Society, Pittsburgh, PA, 1995) p. 633.
[17] R.J. Finch, R.C. Ewing, in: Scientific Basis for Nuclear Waste Management XVI, Materials Research Society Proceedings, Vol. 333, eds. A. Barkatt and R.A. von Konynenburg (Materials Research Society, Pittsburgh, PA, 1994) p. 625.
[18] A. Schoep, Natuurwet. Tijdschr. Ned. Indie 7 (1926) 97.
[19] J.W. Frondel, F. Cuttita, Am. Mineral. 39 (1953) 1018.
[20] A. Schoep, Ann. Mineral. 1, fasc. II (1930) 9.
[21] E.H.P. Cordfunke, G. Prins, P. van Vlaanderen, J. Inorg. Nucl. Chem. 30 (1968) 1745.
[22] J. Cejka, Z. Urbanec, Secondary Uranium Minerals (Academia Nakladatelsvì Ceskoklovenské, Prague, 1990) 93 pp.
[23] P. Taylor, R.J. Lemire, D.D. Wood, in: Proc. 3rd Int. Conf. on High-Level Radioactive Waste Management, Las Vegas, NV (American Nuclear Society, La Grange, IL, and American Society of Civil Engineers, New York, 1992) p. 1442.
[24] P. Taylor, D.D. Wood, D.G. Owen, G.-I. Park, J. Nucl. Mater. 183 (1991) 105.
[25] A. Schoep, S. Stradiot, Am. Mineral. 32 (1947) 344.
[26] C.L. Christ, J.R. Clark, Am. Mineral. 45 (1960) 1026.
[27] R.J. Finch, M.L. Miller, R.C. Ewing, Radiochim. Acta 58&59 (1992) 433.
[28] D.T. Cromer, J.B. Mann, Acta Crystallogr. A24 (1968) 321.
[29] D.T. Cromer, D. Liberman, J. Chem. Phys. 53 (1970) 1891.
[30] H.T. Evans Jr., Science 141 (1963) 154.
[31] P.C. Burns, F.C. Hawthorne, R.C. Ewing, Can. Miner. (1997), accepted.
[32] R.D. Shannon, Acta Crystallogr. A32 (1976) 751.
[33] N.E. Brese, M. O'Keeffe, Acta Crystallogr. B47 (1991) 192.
[34] P.C. Burns, M.L. Miller, R.C. Ewing, Can. Miner. 34 (1996) 845.
[35] B.O. Loopstra, Acta Crystallogr. B26 (1970) 656.
[36] M.K. Pagoaga, D.E. Appleman, J.M. Stewart, Am. Mineral. 72 (1987) 1230.
[37] R.J. Finch, M.A. Cooper, F.C. Hawthorne, R.C. Ewing, Can. Miner. 34 (1996) 1071.
[38] P. Piret, Bull. Miner. 108 (1985) 659.
[39] P.C. Burns, M.L. Miller, R.C. Ewing, J. Nucl. Mater. 245 (1997) 1.
[40] G.G. Christoph, A.C. Larson, P.G. Eller, I.D. Purson, J.D. Zahrt, R.A. Penneman, G.H. Rinehart, Acta Crystallogr. B44 (1988) 575.
[41] T.L. Walker, Am. Mineral. 8 (1923) 67.
[42] Larsen and Berman, 'The microscopic determination of the nonopaque minerals', US Geolog. Survey Bull. 848 (1934).